Research in Astronomy and Astrophysics, 22:065021 (13pp), 2022 June https://doi.org/10.1088/1674-4527/ac6aa9


# Phenol in High-mass Star-forming Regions

Rana Ghosh[1], Milan Sil[2,1], Suman Kumar Mondal[1], Prasanta Gorai[3], Dipen Sahu[4], Rahul Kumar Kushwaha[5], Bhalamurugan Sivaraman[6], and Ankan Das[1]
[1] Indian Centre for Space Physics, 43 Chalantika, Garia Station Road, Kolkata 700084, India; ankan.das@gmail.com
[2] S. N. Bose National Centre for Basic Sciences, Salt Lake, Kolkata 700106, India
[3] Department of Space, Earth & Environment, Chalmers University of Technology, SE-412 96 Gothenburg, Sweden
[4] Institute of Astronomy and Astrophysics Academia Sinica Taipei, Taipei 10617, China
[5] Atomic and Molecular Physics Laboratory, Institute for Nuclear Research (Atomki), Debrecen H-4026, Hungary
[6] Physical Research Laboratory, Navrangpura, Ahmedabad 380009, India
*Received 2022 March 13; accepted 2022 April 11; published 2022 June 6*

## Abstract

Phenol, which belongs to the $C_6H_6O$ isomeric group, is the simplest molecule in the family of alcohol of the aromatic series. Although phenol has yet to be detected in the interstellar medium, a tentative identification was reported toward the Orion KL hot core using the IRAM-30 m line survey. To explore some more species of this isomeric group, we consider ten species to study the fate of their astronomical detection. It is noticed that phenol is the most energetically favorable isomer of this group. In contrast, propargyl ether is the least favorable (having relative energy ∼103 kcal $mol^{-1}$ compared to phenol) species of this group. So far, the studies associated with the formation of phenol are heavily concentrated on combustion chemistry. Here, we suggest a few key reactions ($C_6H_6 + OH \rightarrow C_6H_5 + H_2O$, $C_6H_6 + O \rightarrow C_6H_5OH$, $C_6H_6 + H \rightarrow C_6H_5 + H_2$, and $C_6H_5 + OH \rightarrow C_6H_5OH + h\nu$) for the formation of phenol. All these pathways are included in a large gas-grain chemical network to study its formation in high mass star-forming regions and dark cloud environments. It is noticed that the phenyl ($-C_6H_5$) formation by the ice-phase hydrogen abstraction reaction of benzene (i.e., $C_6H_6 + OH \rightarrow C_6H_5 + H_2O$ if allowed at ∼10 K) could serve as the starting point for the formation of phenol in the gas phase by radiative association reaction $C_6H_5 + OH \rightarrow C_6H_5OH + h\nu$. The gas-phase reaction $C_6H_6 + O \rightarrow C_6H_5OH$ significantly contributes to the formation of phenol, when the ice-phase reaction $C_6H_6 + OH \rightarrow C_6H_5 + H_2O$ is not considered at low temperature. Band 4 ALMA archival data of a hot molecular core, G10.47+0.03, are analyzed. It yields an upper limit on phenol abundance of $5.19 \times 10^{-9}$. Our astrochemical model delivers an upper limit on phenol abundance of $\sim 2.20 \times 10^{-9}$ in the hot molecular core, whereas its production in the dark cloud is not satisfactory.

*Key words:* astrochemistry – ISM: abundances – ISM: molecules – (ISM:) evolution

## 1. Introduction

Theoretically, the presence of aromatic molecules in the interstellar medium (ISM) has yet to be fully understood. However, the recent discovery of benzonitrile (c − $C_6H_5CN$) in a nearby molecular cloud (TMC-1) marks the first radio detection of an aromatic species in the ISM (McGuire et al. 2018). It is suggested that c − $C_6H_5CN$ can be a proxy of benzene (c − $C_6H_6$) at a low-temperature (Cooke et al. 2020), which is the simplest aromatic molecule and plays a significant role in interstellar chemistry. Furthermore, the phenyl radical ($-C_6H_5$) derived from the benzene by a hydrogen abstraction could be a possible progenitor of the formation of other new aromatic species. Various cyclic hydrocarbons, such as ethynyl cyclopropenylidene (c − $C_3HCCH$), cyclopentadiene (c − $C_5H_6$), and indene (c − $C_9H_8$), in the cold dark cloud TMC-1 were recently discovered (Burkhardt et al. 2021; Cernicharo et al. 2021a). Later on, two isomers of ethynyl cyclopentadiene (c − $C_5H_5CCH$) were detected and a tentative detection of ethynyl benzene ($C_6H_5CCH$) was reported by Cernicharo et al. (2021b). Various other cyclic cyano derivatives were observed by Lee et al. (2021), McCarthy et al. (2021), McGuire et al. (2021). It is astonishing to see the presence of such cyclic hydrocarbons in a cold starless region like TMC-1. It imposes a new challenge to reconstruct a chemical model to explain their observed abundances.

Phenol ($C_6H_5OH$) belongs to the alcohol family in aromatic series. It contains the hydroxyl ($-OH$) group directly to the $sp^2$ hybridized carbon atom of the aromatic phenyl ring. Due to the internal rotation of the $-OH$ group, it becomes an exciting candidate to explore from an astrochemist's point of view. The microwave spectrum of phenol was initially measured by Kojima (1960) in the frequency range of 15–30 GHz. Later on, Forest & Dailey (1966) determined the equilibrium structure of phenol by analyzing the rotational spectra of $C_6H_5^{18}OH$, $C_6D_5OH$, and $C_6D_5OD$ within the frequency range of 20–30 GHz. The behavior of phenol and its isomers in the gas phase was examined by Neutralization—Reionization mass

spectrometry (Turecek et al. 1989). Ravi et al. (1998) obtained information about the anomalous temperature dependency of adsorption of phenol. They also concluded that phenol's adsorption and desorption behavior in lower concentrations is quite different from the higher concentration region. Parker & Davis (1999) studied the photochemical reaction between benzene and an oxygen atom ($^3$P) in a solid argon matrix at 12 K. The ultraviolet (UV) light with wavelength $\geqslant$280 nm was used for this study. They obtained phenol, cyclohexadienone, benzene oxide, and butadienylketene as products. Isomerization of phenol is considered an important step in the metabolism of aromatic compounds. Phenol can isomerize to cyclohexadienone by isodesmic reaction with a relative enthalpy of the transition state (TS, 18.6 kcal mol$^{-1}$, which is determined by $\Delta H_{rxn}$ of the isodesmic reaction) over a 69.4 kcal mol$^{-1}$ barrier. This is lower than the energy needed (86 kcal mol$^{-1}$) for phenoxy-H bond cleavage (Zhu & Bozzelli 2003). The millimeter-wave spectra of phenol in the vibrational ground state and the first excited states of the bending and torsion vibrational modes have been studied by Kolesniková et al. (2013). They reported a tentative detection for phenol in the IRAM 30 m line survey of Orion KL. A recent experiment by Rahul et al. (2020) found infrared attenuation due to phase change from amorphous to crystalline in the propargyl ether ices which belong to the same $C_6H_6O$ isomeric group.

In this paper, we study ten molecules belonging to the $C_6H_6O$ isomeric group. The formation of phenol in high-mass star-forming regions and starless dark cloud regions is studied. Atacama Large Millimeter/submillimeter Array (ALMA) archival data of a hot molecular core, G10.47+0.03 (hereafter G10), are analyzed to identify the possible transitions of phenol in this source. Based on the local thermodynamic equilibrium (LTE) analysis, an upper limit on the abundance of phenol is predicted in G10. Upper limit calculations are vital for predicting future detections of complex organic molecules (COMs), including prebiotic molecules (Sahu et al. 2020), and inferring reaction pathways and reaction rates. The paper is organized as follows. In Section 2, for the search of phenol, we explore the band 4 ALMA archival data of G10. How phenol could form is addressed in Section 3. Section 4 discusses the astrochemical model and finally, in Section 5, we conclude. An appendix section (Appendix) is presented to show the thermodynamical parameters of the $C_6H_6O$ isomeric group.

## 2. Astronomical Search for Phenol

Phenol has yet to be detected in the ISM, however, a tentative detection was reported by Kolesniková et al. (2013) in Orion KL. The tentative detection was based on the IRAM 30 m line survey, in the spectral range of 140–170 and 280–360 GHz toward Orion KL. They estimated a column density of $(8 \pm 4) \times 10^{14}$ cm$^{-2}$ (abundance $\sim 8.0 \times 10^{-9}$, considering $N(H_2) = 1.0 \times 10^{23}$ cm$^{-2}$ in Orion KL; Tercero et al. 2011). G10 is another hot core source where many COMs are already reported (Rolffs et al. 2011; Gorai et al. 2020; Mondal et al. 2021). The Orion KL and G10 are both Galactic high-mass star-forming regions. Based on the recent identifications of various alcohols (Mondal et al. 2021) in G10, we search for the simplest alcohol of the aromatic family, phenol in G10. More specifically, we search for the transitions of phenol in ALMA cycle 4 archival data of the hot molecular core G10 (project code #2016.1.00929.S). A detailed description of the data can be found in Gorai et al. (2020), Mondal et al. (2021).

To check the detectability of phenol in G10, we generate synthetic spectra of phenol utilizing the CASSIS spectrum analyzer (Vastel et al. 2015). Here, we use the ALMA telescope to generate the synthetic spectra with a hydrogen column density $\sim 1.35 \times 10^{25}$ cm$^{-2}$ (Gorai et al. 2020), full width at half maximum (FWHM) of 6 km s$^{-1}$, source size of 2″, systematic velocity of 68 km s$^{-1}$, and excitation temperature of 150 K. Mondal et al. (2021) estimated an average rotational temperature of 177 K for various COMs in G10, Olmi et al. (1996) estimated a temperature of about 160 K, and Rolffs et al. (2011) considered 200 K in obtaining the column density of the species identified in G10. Generated LTE synthetic spectra along with the observed spectra are depicted in Figures 1 and 2.

Data presented in Figure 8 of Kolesniková et al. (2013) demonstrate that the transition at 148.489 GHz ($E_{up} = 151.02$ K) has a tentative match with the observed data. A green vertical line in the topmost panel of Figure 1 represents this transition. We notice that this transition is blended with some other transitions of phenol along with a transition of glycolonitrile ($HOCH_2CN$). We vary the abundance of phenol to match this transition. We find that an abundance $\sim 5.19 \times 10^{-9}$ is needed to match the observed intensity. Some transitions (148.6068, 148.9386, 149.2565, and 159.3413 GHz) are marked with blue vertical lines which might have appeared due to phenol, but no conclusive transitions are obtained.

## 3. Kinetics of Phenol

In the Appendix, we present some thermodynamic parameters of the species belonging to the $C_6H_6O$ isomeric group.

### 3.1. At High-temperatures

Benzene and phenol are two fundamental species in the field of combustion chemistry. Zhu & Bozzelli (2003) studied the addition of a hydroxyl radical to benzene. They noticed that it could initially form hydroxyl-cyclohexadienyl, further dissociating to either (i) $C_6H_5OH + H$ or back to (ii) $C_6H_6 + OH$. They considered the overall reaction to phenol to be thermoneutral. Thus, it is at equilibrium under the combustion/high-temperature condition, and hence the thermal

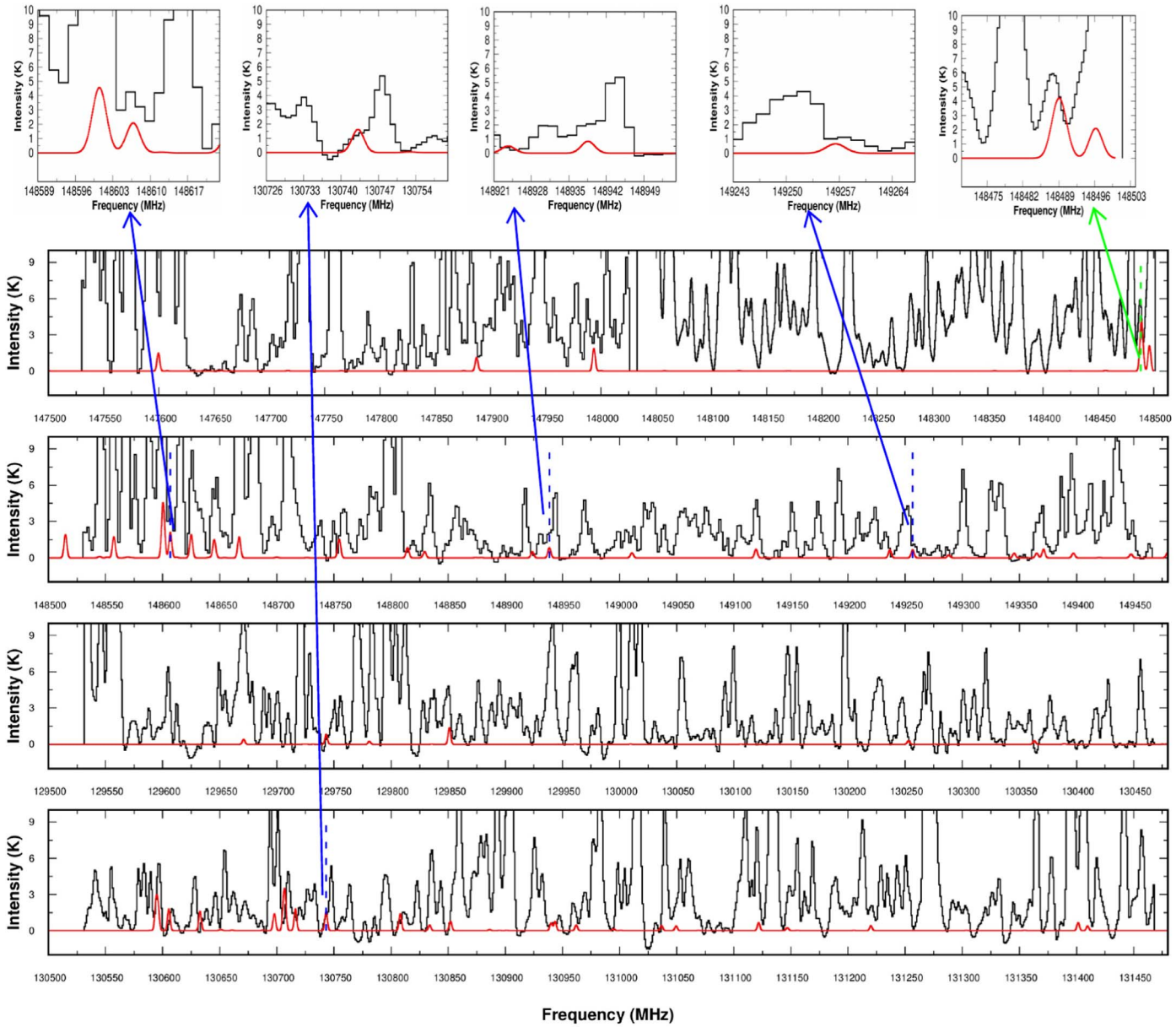


**Figure 1.** Black lines represent the observed spectra toward G10. LTE spectra are shown in red considering $N(H_2) = 1.35 \times 10^{25}$ cm$^{-2}$, excitation temperature = 150 K, source size of 2″, FWHM = 6.0 km s$^{-1}$, and abundance of $5.19 \times 10^{-9}$ (column density = $7.0 \times 10^{16}$ cm$^{-2}$). The green dashed lines indicate the tentatively detected phenol transitions in Orion KL (Kolesniková et al. 2013). The blue dashed lines signify the possible phenol transitions in G10. Solid colored arrows point out enlarged views of the lines.

reaction rate would depend on the concentration of reactant species. Madronich & Felder (1985) applied the AeroChem high-temperature photochemistry technique to study the reaction between $C_6H_6$ and OH over a temperature range of 790–1410 K. Their mechanistic studies around 1300 K showed the following abstraction reactions as a dominant channel

$$C_6H_6 + OH \rightarrow C_6H_5 + H_2O. \quad (1)$$

The rate constant for the reaction of an OH radical with benzene and toluene was measured by Seta et al. (2006). They applied a shock tube/pulsed laser-induced fluorescence imaging method at high temperatures (∼700–1900 K).

Seta et al. (2006) carried out Quantum chemical calculations with G3(MP2)/B3LYP and CBS-QB3 models to resolve the disagreement of the rate constants above a temperature of 500 K between the TS calculations and experiments. They found

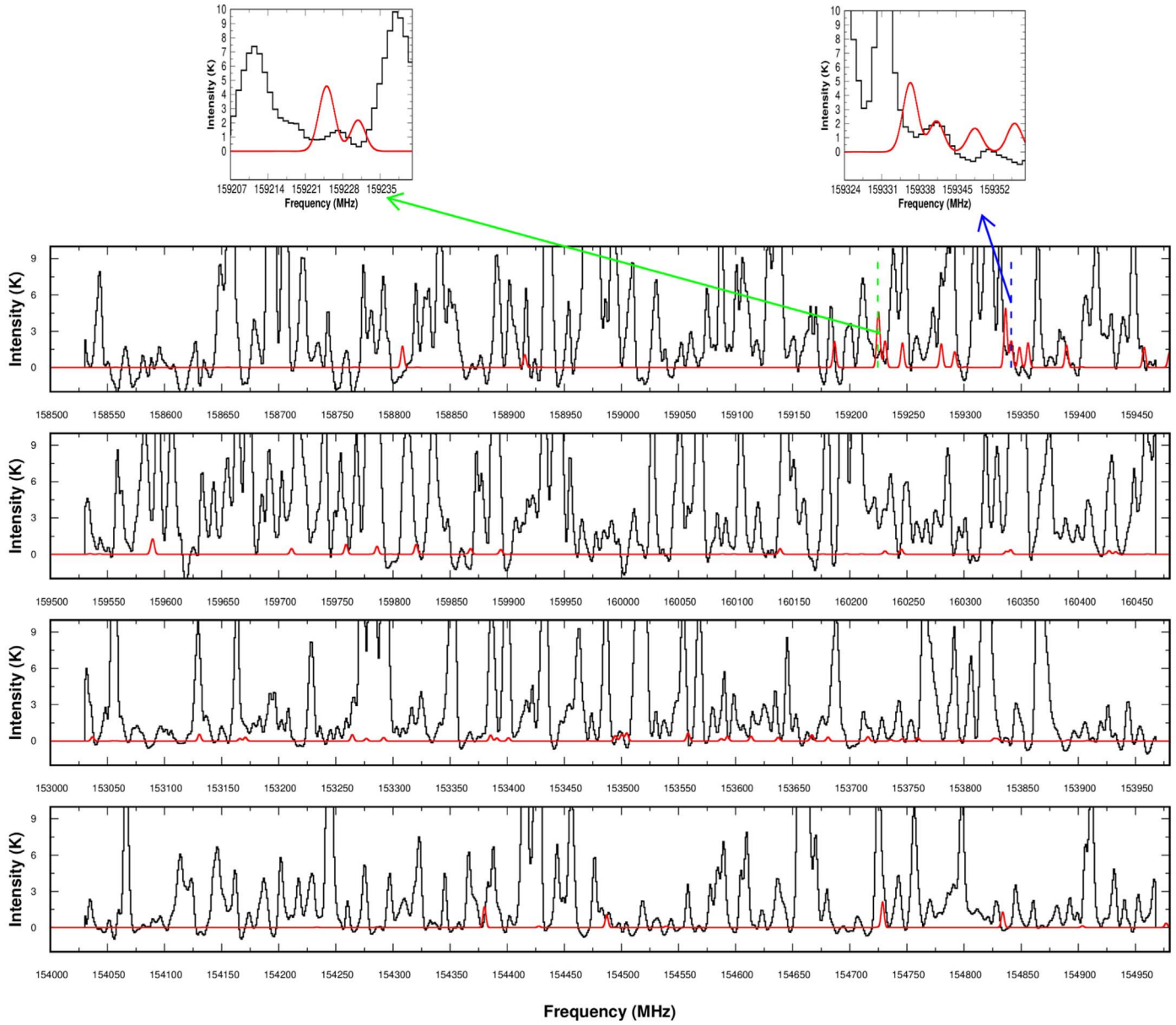


**Figure 2.** Same as Figure 1.

that the discrepancy possibly arises due to the overestimated partition function of the TS. This overestimation happens because of the improper harmonic oscillator approximation of C–H–O wagging, C–H–O rocking, and −OH torsion. Finally, they noted that the anharmonicity of the C–H–O bending vibration plays an important role in reproducing the experimental rate constant by TS theory. They concluded that the H atom abstraction channel (reaction (2)) dominates their temperature range. However, Tokmakov & Lin (2002) indicated that the direct formation of phenol with an H atom abstraction from reaction (2) is negligible over the temperature region 200−2500 K

$$C_6H_6 + OH \rightarrow C_6H_5OH + H. \quad (2)$$

### 3.2. At Interstellar Conditions

The formation pathways discussed above are mostly relevant for combustion chemistry. However, reaction (1), considered by Baulch et al. (2005), could be possible in the temperature range of 298−1500 K. The rate constants $\alpha$, $\beta$, and $\gamma$ of this reaction are considered as $2.8 \times 10^{-11}$, 0, and 2300, respectively.

In the dark cloud region, benzene abundance could reach $\sim 10^{-10}$ (Jones et al. 2011). It plays a vital role in the formation of aromatic molecules. Parker & Davis (1999) carried out photolysis of benzene and ozone mixture in an argon matrix at 12 K. They found that phenol is the major product of their experiment. It would form by the following reaction,

$$C_6H_6 + O(^3P) \rightarrow C_6H_5OH. \quad (3)$$

The $O(^3P)$ in the experiment appears from the photolysis of ozone. They used UV light of $\geqslant 280$ nm for the irradiation. Taatjes et al. (2010) examined the reaction between benzene and $O(^3P)$ over a temperature range of 300−1000 K and a pressure range of 1−10 Torr. They also did quantum chemical calculations to study the fate of this gas-phase reaction. With the TS calculation, they estimated an activation barrier of 3356 K with $\alpha = 9.23 \times 10^{-10}$, $\beta = -2.6$, and $\gamma = 0$ in the temperature range of 500−1000 K.

Wang & Frenklach (1997) considered the formation of a phenyl radical by the hydrogen abstraction reaction of benzene,

$$C_6H_6 + H \rightarrow C_6H_5 + H_2. \quad (4)$$

They considered $\alpha = 4.15 \times 10^{-10}$, $\beta = 0$, and $\gamma = 8050$ for this gas phase reaction within the temperature limit of 50−200 K. If a modified Arrhenius equation (Wakelam et al. 2010) is used to find out the rate coefficient of this reaction, at 200 K, it has a rate around $\sim 1.4 \times 10^{-27}$ cm$^3$ s$^{-1}$. So, it is quite unlikely to form $-C_6H_5$ by reaction (4) in the gas phase. Instead, if this reaction is considered in the ice phase with an activation barrier of 8050 K, it is possible to produce some $-C_6H_5$ at low temperature. However, this type of reaction can occur at a temperature below 20 K, which is falling outside the temperature limit prescribed by Wang & Frenklach (1997). To check the effect of this ice-phase reaction (4), we study the abundance of phenol in the absence and presence of this reaction.

Once a phenyl radical is produced by reactions (1) and (4), we consider the following radiative association reaction to form phenol

$$C_6H_5 + OH \rightarrow C_6H_5OH + h\nu. \quad (5)$$

We did not find any study which used reaction (5) for the formation of phenol. Vasyunin & Herbst (2013) discussed the radiative association reaction between two radicals ($CH_3O$ and $CH_3$). They proposed a temperature-dependent rate coefficient for such reaction with $\alpha = 10^{-15}$, $\beta = -3.0$, and $\gamma = 0.0$. Sil et al. (2018) also consider similar rate constants for the chemical modeling in predicting the abundances of certain aldimines and amines in hot cores. However, looking at the large uncertainty in the prescribed rate constant, we use $\alpha = 10^{-10}$ for most of the cases to see the upper limit of forming phenol with reaction (5). For some specific cases, we apply the rate constants used in Vasyunin & Herbst (2013).

## 4. Astrochemical Model

Here, Chemical Model of Molecular Cloud is implemented (Das et al. 2019, 2021; Gorai et al. 2020; Mondal et al. 2021; Sil et al. 2021; Bhat et al. 2022) to study the chemical evolution of phenol in high-mass star-forming regions and dark cloud environments.

### 4.1. Hot Core Model

For the high-mass star-forming regions, Gorai et al. (2020), Sil et al. (2021), Mondal et al. (2021) considered three distinct stages, (a) isothermal collapse ($n_H = 3.0 \times 10^3$–$10^7$ cm$^{-3}$, $T_{gas} = T_{ice} = 10$ K, $A_V = 2 - 200$, time $= 10^5$ yr), (b) warm-up ($n_H = 10^7$ cm$^{-3}$, $T_{gas} = T_{ice} = 10$–200 K, $A_V = 200$, time $= 5.0 \times 10^4$ yr), and (c) post-warm-up ($n_H = 10^7$ cm$^{-3}$, $T_{gas} = T_{ice} = 200$ K, $A_V = 200$, time $= 1.0 \times 10^5$ yr). Here, following Garrod et al. (2017), for the isothermal collapse phase, we consider minimum density ($n_{H0}$) $= 3 \times 10^3$ cm$^{-3}$ and maximum density ($n_{Hmax}$) $= 2 \times 10^8$ cm$^{-3}$. A shorter collapsing time ($\sim 10^5$ yr) is considered. Visual extinction parameter is allowed to vary from a minimum value ($A_V = 2$) to $A_V = A_{V0}(n_H/n_{H0})^{2/3}$ (Garrod 2008). Dust temperature is allowed to vary depending on the $A_V$ (Garrod 2008), whereas the gas temperature is kept constant at 10 K. During the initial warm-up phase, the cloud is allowed to warm up (gas and grain both) to 200 K in $10^5$ yr. Then another $2.12 \times 10^4$ yr is used to warm up to 400 K. Finally, another $10^5$ yr is used for the post-warm-up phase, where temperature, density, and visual extinction are kept constant at their respective highest values. So, in total, our simulation continues up to $3.212 \times 10^5$ yr.

Ice-phase pathways are crucial for the chemical complexity of the ISM. Even the abundances of the most abundant species, $H_2$, could not be explained without considering ice-phase chemistry (Biham et al. 2001; Chakrabarti et al. 2006a, 2006b; Sahu et al. 2015). Hydrogenation reactions at the ice phase play a crucial role for the formation of COMs (Hasegawa et al. 1992; Das et al. 2008, 2010, 2016; Das & Chakrabarti 2011). Ice-phase reactions are included following Hasegawa et al. (1992), Ruaud et al. (2015), Das et al. (2015a, 2015b), Gorai et al. (2017a, 2017b). The binding energies of most of the ice phase species are considered following Garrod et al. (2017). For phenyl radical and phenol, we calculate the binding energies by the method prescribed in Sil et al. (2017), Das et al. (2018, 2021). As a result, we obtain binding energy (scaled by 1.416, because we use water monomer as a substrate here) of $C_6H_5$ and $C_6H_5OH$ as 2056 K and 5476 K, respectively.

Since the formation/destruction of nine other species of $C_6H_6O$ except phenol are poorly constrained, their formation/destruction are not considered here. We prepare various models to study the fate of the phenol production in such environments. Models are prepared based on the reactions (1), (3), (4), and (5) (see Table 1). For the destruction of phenol in the gas phase, photodissociation ($\alpha = 2.9 \times 10^{-9}$, $\beta = 0$, and $\gamma = 1.7$ is

**Table 1**
Models Considered in this Study

| Reactions | C1 | C2 | C3 | C4 | C5 | C6 | C7 | C8 | C9 | C10 | DC |
|---|---|---|---|---|---|---|---|---|---|---|---|
| $C_6H_6 + OH \rightarrow C_6H_5 + H_2O$ (1) | | | gas | gas | gas | gas | gas | gas+ice | gas+ice | gas+ice[a] | gas+ice |
| $C_6H_6 + O \rightarrow C_6H_5OH$ (3) | gas | | | gas | gas+ice | gas+ice | gas+ice | gas+ice | gas+ice | gas+ice | gas+ice |
| $C_6H_6 + H \rightarrow C_6H_5 + H_2$ (4) | | gas | | gas | gas | gas+ice | gas+ice | gas+ice | gas+ice | gas+ice[a] | gas+ice |
| $C_6H_5 + OH \rightarrow C_6H_5OH + h\,\nu$ (5) | | gas | gas | gas | gas | gas | gas+ice | gas+ice | gas[b]+ice | gas[b]+ice | gas+ice |
| Peak abundance | $1.67 \times 10^{-12}$ | $1.72 \times 10^{-21}$ | $4.16 \times 10^{-15}$ | $1.67 \times 10^{-12}$ | $1.67 \times 10^{-12}$ | $1.67 \times 10^{-12}$ | $1.67 \times 10^{-12}$ | $2.20 \times 10^{-9}$ | $1.09 \times 10^{-11}$ | $1.67 \times 10^{-12}$ | $9.93 \times 10^{-16}$ |

**Notes.**
[a] Temperature limit considered in gas and ice phase.
[b] used $\alpha = 10^{-15}$ and $\beta = -3.0$ for $C_6H_5 + OH \rightarrow C_6H_5OH + h\nu$ (reaction (5)).

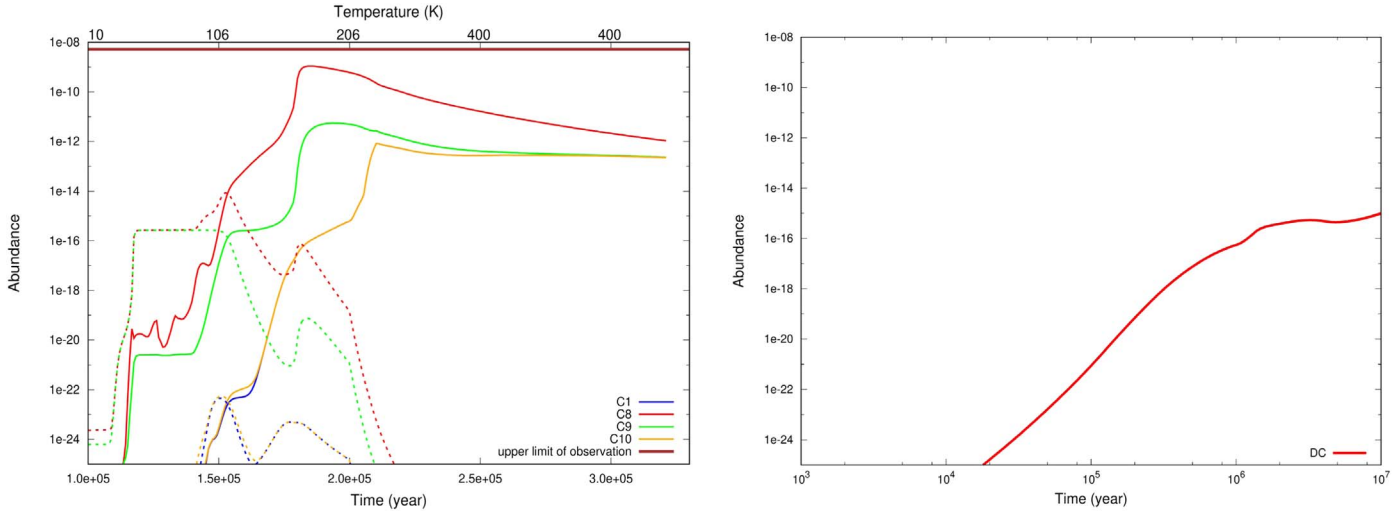


**Figure 3.** The left panel shows the time evolution (during the warm-up and post-warm-up phase) of phenol for some selected models noted in Table 1. Solid lines represent the gas-phase abundance, whereas the ice phase abundance is depicted with dashed curves. The right panel displays the time evolution of gas-phase phenol in a starless dark cloud model.

used) and cosmic ray dissociation ($\alpha = 1.3 \times 10^{-17}$, $\beta = 0$, and $\gamma = 263.5$) are considered. Furthermore, its destruction by the major ions ($C^+$, $He^+$, $HCO^+$, and $H_3O^+$) is also considered.

In Table 1, models C1–C4 are classified based on the gas-phase reactions (1), (3), (4), and (5). Models C1–C4 do not consider any of these four reactions in the ice phase. Following Baulch et al. (2005) and the KIDA database[7], in models C3 and C4, reaction (1) is considered to be valid within a temperature limit of 298−1500 K. For reaction (3), Taatjes et al. (2010) proposed $\gamma = 3356$ K and a temperature window of 500−1000 K. However, Parker & Davis (1999) carried out photolysis at 12 K and found that phenol was produced. Based on the experiment of Parker & Davis (1999), our models C1 and C4 consider reaction (3) at a low temperature (∼10 K) with the gas phase rate constants found by Taatjes et al. (2010). Following Wang & Frenklach (1997), for reaction (4), a temperature window of 50−200 K is considered with $\gamma = 8050$ K in models C2 and C4. Reaction (5) is considered as barrier-less in models C2 and C3 with $\alpha = 10^{-10}$. The abundances noted in Table 1 clearly indicate that the gas-phase reaction (3) is the key if it is considered at low temperature ∼10 K. We have obtained a peak gas-phase abundance of $1.67 \times 10^{-12}$ for phenol among models C1–C4. The left panel of Figure 3 shows the time evolution of phenol beyond the collapsing time. Observed upper limit of phenol abundance is highlighted with the brown horizontal line.

From model C5 onward, these four reactions are sequentially considered in the ice phase with the activation barriers similar to the gas-phase rate constant, $\gamma$. However, for models C5–C9, no temperature restriction of ice-phase reactions is considered. Ice-phase rate constants are calculated by the method described in Hasegawa et al. (1992). From Table 1, it is clear that consideration of the ice-phase reactions (3), (4), and (5) does not increase the formation of phenol. Instead, ice-phase reaction between $C_6H_6$ and −OH (reaction (1)) is contributing (see abundance obtained from model C8). This is a hydrogen abstraction reaction. Following Belloche et al. (2016), Garrod et al. (2017), here also, we consider the hydrogen mass instead of the reduced mass to calculate the tunneling rate of this reaction. The other hydrogen abstraction reactions of Belloche et al. (2016), Garrod et al. (2017) are also considered in our model. With the consideration of the ice-phase reaction (1), we have obtained a peak gas-phase abundance of phenol as $2.20 \times 10^{-9}$. The models C8 and C9 are the same, except for the gas-phase rate constants considered for reaction (5). In model C9, we have considered $\alpha = 10^{-15}$ and $\beta = -3.0$ instead of $\alpha = 10^{-10}$ and $\beta = 0$ applied in model C8. With the consideration of the lower leading rate constant, phenol abundance drops to $1.09 \times 10^{-11}$. The left panel of Figure 3 plots the time evolution of phenol with models C8 and C9.

A separate model C10 is constructed by implementing the temperature limit of the reactions (1) and (4) in both the gas and ice phases. For the gas-phase reaction (5), the rate constant ($\alpha = 10^{-15}$, $\beta = -3.0$, and $\gamma = 0$) mentioned in the context of model C9 is utilized. Reaction (3) is considered to be valid ∼10 K. The orange line of the left panel of Figure 3 shows the time evolution of gas-phase phenol obtained with model C10. The peak abundance obtained with this model is $1.67 \times 10^{-12}$ for this. So, if the ice-phase hydrogen abstraction reaction (1) is not considered at low temperature, then the gas-phase reaction (3) controls the formation of phenol.

[7] http://kida.astrophy.u-bordeaux

### 4.2. Dark Cloud Model

Benzonitrile was observed in a starless dark cloud, TMC-1 (McGuire et al. 2018). This might have formed by the reaction between the benzene and cyanide (−CN) radical. A similar pathway for the formation of phenol is considered here (reaction (5)). For the dark cloud model DC, some standard parameters are implemented ($n_{\rm H} = 2.0 \times 10^4$ cm$^{-3}$, $T_{\rm gas} = T_{\rm ice} = 20$ K, $A_V = 10$, time $= 1.0 \times 10^7$ yr). The right panel of Figure 3 represents the time evolution of phenol for the dark cloud condition. It is clear from the figure that even with the highest rate constant and avoiding the temperature restriction, we can have a maximum gas-phase abundance of $9.93 \times 10^{-16}$ for phenol.

## 5. Conclusions

Interstellar chemistry is far from equilibrium, and the reaction pathways mainly control it. However, based on the reaction energy, dipole moment, and enthalpy of formation, it shows that phenol, 2,5-cyclohexadienone, and cyclohexadienone are the probable candidates and propargyl ether (the only non-cyclic structure among all the isomers considered here) is the least probable candidate for future astronomical detection in the $C_6H_6O$ isomeric group. Therefore, we prepare a chemical model to check the fate of the formation of phenol in the high mass star-forming regions (models C1–C10) and dark cloud (model DC) environments. We notice that even with the upper limit of the rate constant and no temperature limitation for the ice-phase reactions, the formation of phenol is inadequate in the dark cloud condition. In contrast, we ascertained the chances of forming phenol in the hot core from our astrochemical model. We found that the ice-phase hydrogen abstraction reaction (if allowed at ∼10 K) of benzene with −OH radical can produce $-C_6H_5$ radical and $H_2O$ on the grain. The $-C_6H_5$ radical eventually transferred to the gas phase to form phenol by the radiative association reaction with −OH radical. With the upper limit of the rate constant of radiative association reaction between $-C_6H_5$ and −OH radicals ($\alpha = 10^{-10}$) along with the hydrogen abstraction reaction of benzene allowed at the low temperature, our model predicts a peak gas-phase abundance of $\sim 2.20 \times 10^{-9}$ for phenol. When a temperature restriction (reaction (1) is considered in gas and ice phase beyond 298 K) is applied and a conservative rate constant for the radiative association reaction is used, reaction (1) becomes obsolete and obtains a peak gas-phase abundance $\sim 1.67 \times 10^{-12}$ for phenol, which occurs due to the other gas-phase reaction $C_6H_6 + O \rightarrow C_6H_5OH$ (reaction (3)). All these obtained peak abundances are consistent (below) with the upper limit ($5.19 \times 10^{-9}$) set by the data analysis of a Galactic high-mass star-forming region, G10.

## Acknowledgments

R.G. wants to acknowledge the SVMCM scholarship, Government of West Bengal. M.S. [IF160109] gratefully acknowledges the DST-INSPIRE Fellowship scheme for financial assistance. S.K.M. (09/904(0014)/2018-EMR-I) acknowledges the CSIR fellowship. This paper makes use of the following ALMA archival data: ADS/JAO. ALMA#2016.1.00929.S. (ALMA is a partnership of ESO (representing its member states), NSF (USA) and NINS (Japan), together with NRC (Canada), MOST and ASIAA (Taiwan), and KASI (Republic of Korea), in cooperation with the Republic of Chile. The Joint ALMA Observatory is operated by ESO, AUI/NRAO and NAOJ).

## Appendix
## Thermodynamic Data of $C_6H_6O$ Isomeric Group

To carry out a comprehensive study of thermodynamic data among the ten considered species from $C_6H_6O$ isomeric group, we perform quantum chemical calculations using the Gaussian 09 suite of programs (Frisch et al. 2013). Out of the ten considered isomers of phenol, nine are cyclic. Only propargyl ether is not a cyclic member. The optimized structures (see Figure A1) are subsequently characterized by the harmonic vibrational analysis.

### A.1. Electronic Energy with Zero-point Vibrational Energy Correction

The electronic energy values with zero-point vibrational energy correction ($E_0$+ZPVE) for all the species are calculated. The G4 composite method (Curtiss et al. 2007) is utilized for these computations. These values are arranged in descending order in Table A1. The relative energy value of a species is calculated by subtracting their $E_0$+ZPVE from that of the phenol (see the bracketed term of column 3 in Table A1). The equilibrium geometry of all the optimized structures is verified based on the non-negative frequencies of vibration. This allows all the species to locate them at the valley on the potential energy surface. According to our calculations, phenol is energetically most favorable, and propargyl ether is the least favorable candidate of the $C_6H_6O$ isomeric group. We notice that the relative energy of 2,5-cyclohexadienone is greater than that of phenol by ∼17 kcal mol$^{-1}$. Cyclohexadienone is the third in this series, having relative energy ∼18 kcal mol$^{-1}$ compared to phenol. Le et al. (2001) carried out the quantum chemical calculations with B3LYP/6-311++G(d,p) + ZPVE. They found that cyclohexadienone and 2,5-cyclohexadienone have the relative energies of 17.4 kcal mol$^{-1}$ and 16.5 kcal mol$^{-1}$, respectively compared to phenol. The gas-phase tautomerism process of phenol has been attempted by Gómez et al. (2006) theoretically by using Gaussian 03 suite of quantum-chemical programs. They showed that phenol is more

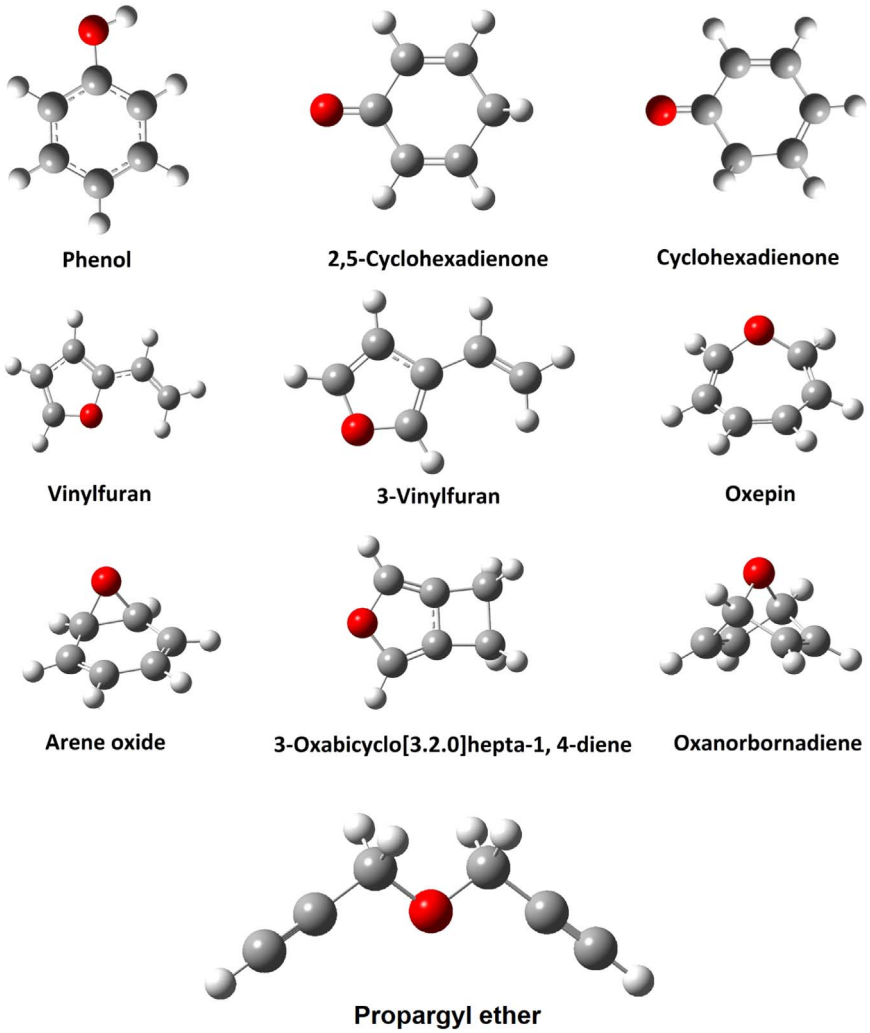


**Figure A1.** The optimized structures of $C_6H_6O$ isomeric group. Except propargyl ether, all the isomers are cyclic.

stable than its tautomers (cyclohexadienone and 2,5-cyclohexadienone). It is noticed that phenol is more stable by 19.1 kcal mol$^{-1}$ and 17.2 kcal mol$^{-1}$ than cyclohexadienone and 2,5-cyclohexadienone, respectively. Moreover, Gómez et al. (2006) predicted that 2,5-cyclohexadienone is energetically lower (by 1.9 kcal mol$^{-1}$) than cyclohexadienone. They used the CASPT2(8,8)/cc-pVDZ level of theory for energy calculation and CASSCF(8,8)/6-31G(d) level of theory for geometry optimization. Our calculations noted in Table A1 report a ∼1 kcal mol$^{-1}$ energy difference between these two.

### *A.2. Enthalpy of Formation*

We include the calculated enthalpy of formation ($\Delta_f H^0$) of these species by using Density Functional Theory (DFT) with the popular hybrid B3LYP functional and 6-31G(d,p) basis set. The obtained $\Delta_f H^0$ are compared with the experimental values (if available). The enthalpy of formation denotes the enthalpy changes, accompanied by the formation of a species from its constituents. Table A1 shows a negative value for the first three species, and the rest are positive. The negative value refers to the exothermicity, where energy is usually released to form a stronger bond. On the contrary, the positive value refers to the thermodynamically least favorable endothermicity under the interstellar condition. However, it is essential to note that interstellar chemistry is far from equilibrium, and kinetics dominate the chemical composition rather than thermodynamics. Our calculations demonstrate that phenol releases ∼22 kcal mol$^{-1}$, whereas 2,5-cyclohexadineone and cyclohexadineone release ∼5 kcal mol$^{-1}$ and 4 kcal mol$^{-1}$, respectively to form the bond. Zhu & Bozzelli (2003) calculated the standard enthalpy of formation value of cyclohexadienone and 2,5-cyclohexadienone by applying CBS-QB3 level of theory. Their finding is similar to our values ($-4.4 \pm 2.4$ kcal mol$^{-1}$ and

**Table A1**
The Enthalpy of Formation at 298 K, Electronic Energy ($E_0$) with Zero-point Vibrational Energy (ZPVE), and Relative Energy with the G4 Composite Method for ten Species of the $C_6H_6O$ Isomeric Group

| Serial No. | Species | $E_0$+ZPVE in Hartree/Particle (Relative Energy in kcal mol$^{-1}$) | Calculated $\Delta_f H^0$ at $T = 298$ K Using G4 Composite Method (Using B3LYP/6-31G(d,p) Method) (in kcal mol$^{-1}$) | Experimental $\Delta_f H^0$ at $T = 298$ K (in kcal mol$^{-1}$) |
|---|---|---|---|---|
| 1 | Phenol | −307.387662 (0.000000) | −22.047392 (−17.587071) | −23.03[a] |
| 2 | 2,5-cyclohexadienone | −307.360965 (16.751369) | −5.182519 (−1.506103) | −11.95[a], −6.0 ± 2.4[b] |
| 3 | cyclohexadienone | −307.359278 (17.810605) | −4.010040 (−0.623054) | −4.4 ± 2.4[b] |
| 4 | Vinylfuran | −307.348834 (24.364315) | 2.561879 (7.520718) | 6.6444[c] |
| 5 | 3-Vinylfuran | −307.341343 (29.06499) | 7.461043 (12.307825) | |
| 6 | Oxepin | −307.317155 (44.243192) | 22.318538 (27.000497) | |
| 7 | Arene Oxide | −307.313922 (46.271931) | 24.015868 (28.049861) | |
| 8 | 3-Oxabicyclo[3.2.0]hepta-1, 4-diene | −307.299106 (55.569113) | 33.377396 (37.848077) | |
| 9 | Oxanorbornadiene | −307.281912 (66.358513) | 43.830,071 (48.037668) | |
| 10 | Propargyl Ether | −307.223585 (102.959266) | 82.496958 (90.075299) | |

**Notes.**
[a] https://cccbdb.nist.gov
[b] Zhu & Bozzelli (2003).
[c] Lide (2004).

$-6.0 \pm 2.4$ kcal mol$^{-1}$ for cyclohexadienone and 2,5-cyclohexadienone, respectively). Table A1 affirms that the calculated $\Delta_f H^0$ for phenol with the G4 composite method ($-22.04$ kcal mol$^{-1}$) is in good agreement with the experiment ($-23.03$ kcal mol$^{-1}$). With the DFT-B3LYP/6-31G(d,p) level of theory, we obtain a large deviation from the experimental values. Zhu & Bozzelli (2003) also showed that their results in obtaining the value of $\Delta_f H^0$ at 298 K are significantly higher than the experimentally determined $\Delta_{f,298} H^0$ values of Shiner et al. (1986) for cyclohexadineone and 2,5-cyclohexadienone. But, the trend we are getting in our calculation is the same as that of Le et al. (2001), Gadosy & McClelland (1996), Zhu et al. (2000), Santoro & Louw (2001), i.e., $\Delta_{f,298} H^0$ (phenol) $\ll \Delta_{f,298} H^0$ (2,5-cyclohexadienone) $< \Delta_{f,298} H^0$(cyclohexadienone). A graphical representation of enthalpy of formation is displayed in Figure A2. It depicts that the relative energy of propargyl ether is the highest in between this isomeric group (∼103 kcal mol$^{-1}$).

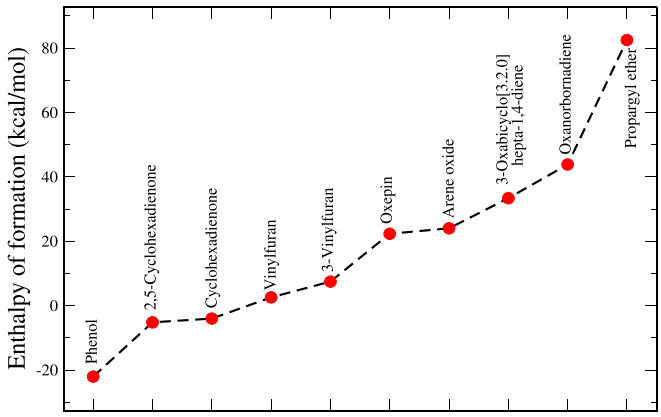


**Figure A2.** Enthalpy of Formation for different species in $C_6H_6O$ isomeric group.

### *A.3. Dipole Moment Components*

Radio astronomy is the most powerful tool to identify interstellar species. It already bears ∼200 species (including radicals and ions) in the ISM. The intensity of a rotational transition between two rotational energy levels may change due to the relative sign of the dipole moment components (a-type, b-type, and c-type) that are small in magnitude (Müller et al. 2016). The expected intensities are directly proportional to the square of the total dipole moment ($\mu_{\rm total}$) of that species and inversely proportional to the rotational partition function ($Q_{\rm rot}$) at a particular temperature. So, at a fixed temperature, the higher the value of the total dipole moment is, higher the intensities. Dipole moments in the unit of debye of each species along the fixed *a*-, *b*- and *c*-axis ($\mu_a$, $\mu_b$, and $\mu_c$) and the total dipole moment ($\mu_{\rm total}$) are noted in Table A2. To calculate the dipole moment of this isomeric group, we use the DFT-B3LYP/6-31G(d,p) level of quantum chemical theory. The experimental values (if available) are also noted in parentheses. They show that our calculated values can successfully explain the experimentally obtained values. The size and direction of a species could characterize the dipole moment. Here, from our calculations, we obtain a total dipole moment of phenol as 1.3359 D, which is in good agreement with the available literature values (McClellan 1963; Johnson 1999; Reese et al. 2004). In the case of Vinylfuran, "c" type transition is absent,

**Table A2**
Calculated Dipole Moment Components for Ten Species of the $C_6H_6O$ Isomeric Group with DFT/B3LYP 6-31G(d,p) Method

| Serial No. | Species | $\mu_a$(D) | $\mu_b$(D) | $\mu_c$(D) | $\mu_{total}$(D) |
|---|---|---|---|---|---|
| 1 | Phenol | 0.0946 ($-0.133 \pm 0.003$)[a] | 1.3326 ($1.217 \pm 0.008$)[a] | 0.0000 (0.000)[a] | 1.3359 ($1.224 \pm 0.008$)[a], 1.45[b] |
| 2 | 2,5 -cyclohexadienone | 4.4575 | 0.0005 | 0.0001 | 4.4575 |
| 3 | cyclohexadienone | −3.4890 | 0.4296 | −0.0011 | 3.5154 |
| 4 | Vinylfuran | −0.6237 | 0.4933 | 0.0000 | 0.7952 ($0.69 \pm 0.07$)[c] |
| 5 | 3-Vinylfuran | 0.1191 | 0.5266 | −0.0090 | 0.5400 |
| 6 | Oxepin | 0.5949 | 0.0000 | −1.2178 | 1.3554 |
| 7 | Arene Oxide | −0.9200 | −0.0006 | −1.7205 | 1.9510 |
| 8 | 3-Oxabicyclo[3.2.0]hepta-1,4-diene | −1.3382 | 0.0001 | −0.0033 | 1.3382 |
| 9 | Oxanorbornadiene | 0.0000 | 0.0000 | −1.8709 | 1.8709 |
| 10 | Propargyl Ether | −0.0003 | 1.5289 | 0.0005 | 1.5289 |

**Notes.** Experimental values are noted in parentheses (if available).
[a] Johnson (1999).
[b] McClellan (1963).
[c] Lide (2004).

**Table A3**
Calculated Rotational Constant and Rotational Partition Function ($Q_{rot}$) at 150 K for Ten Species of the $C_6H_6O$ Isomeric Groups with the MP2/6-311G++(d,p) Method

| Serial No. | Species | *A* (in MHz) | *B* (in MHz) | *C* (in MHz) | Rotational Partition Function at 150 K |
|---|---|---|---|---|---|
| 1 | Phenol | 5627.92 (5650.52)[a] | 2605.76 (2619.24)[a] | 1781.25 (1789.85)[a] | 0.605,968(+05) |
| 2 | 2,5-cyclohexadienone | 5226.05 (5228)[b] | 2652.04 (2653)[b] | 1778.26 (1779)[b] | 0.623,848(+05) |
| 3 | cyclohexadienone | 5127.57 | 2693.12 | 1805.09 | 0.620,327(+05) |
| 4 | Vinylfuran | 7811.41 | 2103.65 | 1657.32 | 0.593,470(+05) |
| 5 | 3-Vinylfuran | 7785.52 | 1955.09 | 1599.18 | 0.627,738(+05) |
| 6 | Oxepin | 4030.06 | 3817.33 | 2145.01 | 0.539,143(+05) |
| 7 | Arene oxide | 4552.69 | 3588.31 | 2304.04 | 0.504,812(+05) |
| 8 | 3-Oxabicyclo[3.2.0]hepta-1,4-diene | 6714.63 | 2711.64 | 1980.23 | 0.515,786(+05) |
| 9 | Oxanorbornadiene | 4527.55 | 3722.71 | 3301.26 | 0.207,598(+05) |
| 10 | Propargyl ether | 11,416.16 | 1056.99 | 979.71 | 0.900,761(+05) |

**Notes.**
[a] Larsen (1979).
[b] Johnson (1999).

and the total calculated electric dipole moment (0.7952 D) shows good agreement with the available value (0.69 D; Lide 2004). In oxanorbornadiene, the "a" and "b" type rotational transition is absent, whereas the "c" type transition is available.

### *A.4. Rotational Constants*

No microwave spectra of a species are observed unless it has a permanent electric dipole moment. The intensity of spectra depends on the shape of a species. Quantum chemical studies can provide a reliable spectroscopic constant (comparable to experimental value) to aid laboratory microwave studies. These studies are essential as these could ultimately lead to the identification of new species in the ISM. So, a high level of quantum chemical theory is needed for a precise calculation of rotational spectroscopic parameters. Here, Møller–Plesset of second order perturbation (MP2) method (Møller & Plesset 1934), with the 6-311G++(d,p) including a diffuse function are used to calculate the rotational constants (*A*, *B*, and *C*) of the species of $C_6H_6O$ isomeric group (see Table A3). The obtained values are compared with the experimentally obtained parameters (if available). The comparison between these two data shows that calculated values are matched well with the experimentally obtained values.

$\mu_b^2/Q_{rot}$ would indicate the expected antenna temperature of some large molecules (Charnley et al. 1995). They used b-type electric dipole moment because it was much more extensive for all types of molecules considered in their study. For our

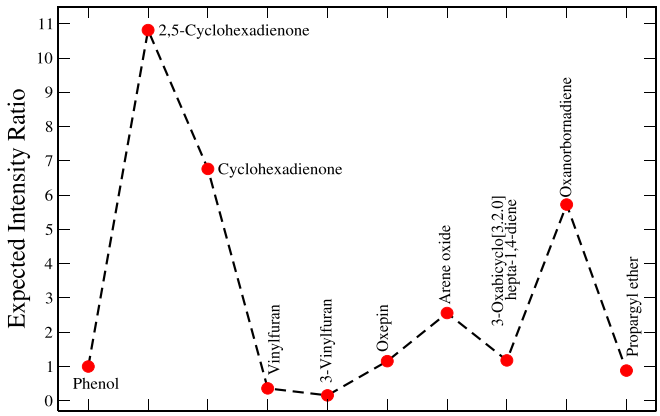


**Figure A3.** Expected intensity ratio of the $C_6H_6O$ isomeric groups.

molecules (belonging to the $C_6H_6O$ isomeric group), we did not see any such trend for any specific type of dipole moment. Therefore, we use the total dipole moment ($\mu_{\rm total}$) for our case rather than relying on a particular kind of dipole moment. Figure A3 features a comparative study on the expected antenna temperature of the $C_6H_6O$ isomeric group. Only the ${\mu_{\rm total}}^2/Q_{\rm rot}$ is considered for this comparison. In reality, the intensity would also depend on the abundance, which is not considered here. It is the reaction pathways that control their abundance. Figure A3 shows that this probability is maximum for 2,5-cyclohexadienone. Rotational constants and rotational partition function for the $C_6H_6O$ isomeric group are listed in Table A3. Rotational constants along the three principal axes ($a$, $b$ and $c$) are given in the unit of MHz. In the case of phenol, the calculated values of rotational constants $A$, $B$, and $C$ are 5627.92 MHz, 2605.76 MHz, and 1781.25 MHz, respectively, and all are approximately well matched with experimental values and have the deviation of 0.4%, 0.5%, and 0.5%, respectively, from the experimental values. We obtain a variation of 0.04%, 0.04%, and 0.02% in the calculated $A$, $B$, and $C$ from the experimental values for 2,5-cyclohexadienone respectively. For the rest of the species, no experimental values are available. So, our calculation would be an essential guideline for the rotational constants of these species. Based on the values obtained for phenol and 2,5-cyclohexadienone, it is expected that our calculated value would have a minor deviation from the experimentally obtained values. Table A3 reports the rotational partition functions for all the isomers at a 150 K temperature relevant for the hot core condition. These values play a significant role to derive the molecular column densities and help to calculate line intensities. These partition functions are calculated quantum chemically applying the "freqchk" utility, which is used to retrieve frequency and thermochemistry data from a checkpoint file, with the optional specification of alternate temperature, pressure, scale factor, and/or isotope substitutions. As all the isomers are asymmetric top molecules, one can reference the approximate ground vibrational state rotational partition function for the asymmetric top molecules (Cernicharo et al. 2016; Sil et al. 2018) using the following relation

$$Q_{\rm rot} = 5.3311 \times 10^6 \sqrt{(T^3/ABC)}/\sigma. \quad \text{(A1)}$$

Here $\sigma$ is the rotational symmetry number having the value 1 for all species, $A$, $B$, and $C$ are the rotational constants for the molecule (in MHz) and $T$ is the temperature (in K).

## ORCID iDs

Rana Ghosh https://orcid.org/0000-0003-1745-9718
Milan Sil https://orcid.org/0000-0001-5720-6294
Suman Kumar Mondal https://orcid.org/0000-0002-7657-1243
Prasanta Gorai https://orcid.org/0000-0003-1602-6849
Dipen Sahu https://orcid.org/0000-0002-4393-3463
Rahul Kumar Kushwaha https://orcid.org/0000-0002-5914-7061
Bhalamurugan Sivaraman https://orcid.org/0000-0002-2833-0357
Ankan Das https://orcid.org/0000-0003-4615-602X

## References

Baulch, D., Bowman, C., Cobos, C. J., et al. 2005, JPCRD, 34, 757
Belloche, A., Müller, H. S. P., Garrod, R. T., & Menten, K. M. 2016, A&A, 587, A91
Bhat, B., Gorai, P., Mondal, S. K., Chakrabarti, S. K., & Das, A. 2022, AdSpR, 69, 415
Biham, O., Furman, I., Pirronello, V., & Vidali, G. 2001, ApJ, 553, 595
Burkhardt, A. M., Lee, K. L. K., Changala, P. B., et al. 2021, ApJL, 913, L18
Cernicharo, J., Agúndez, M., Cabezas, C., et al. 2021a, A&A, 649, L15
Cernicharo, J., Agúndez, M., Kaiser, R. I., et al. 2021b, A&A, 655, L1
Cernicharo, J., Kisiel, Z., Tercero, B., et al. 2016, A&A, 587, L4
Chakrabarti, S. K., Das, A., Acharyya, K., & Chakrabarti, S. 2006a, A&A, 457, 167
Chakrabarti, S. K., Das, A., Acharyya, K., & Chakrabarti, S. 2006b, BASI, 34, 299
Charnley, S. B., Kress, M. E., Tielens, A. G. G. M., & Millar, T. J. 1995, ApJ, 448, 232
Cooke, I. R., Gupta, D., Messinger, J. P., & Sims, I. R. 2020, ApJL, 891, L41
Curtiss, L. A., Redfern, P. C., & Raghavachari, K. 2007, JChPh, 126, 084108
Das, A., Acharyya, K., Chakrabarti, S., & Chakrabarti, S. K. 2008, A&A, 486, 209
Das, A., Acharyya, K., & Chakrabarti, S. K. 2010, MNRAS, 409, 789
Das, A., & Chakrabarti, S. K. 2011, MNRAS, 418, 545
Das, A., Gorai, P., & Chakrabarti, S. K. 2019, A&A, 628, A73
Das, A., Majumdar, L., Chakrabarti, S. K., & Sahu, D. 2015a, NewA, 35, 53
Das, A., Majumdar, L., Sahu, D., et al. 2015b, ApJ, 808, 21
Das, A., Sahu, D., Majumdar, L., & Chakrabarti, S. K. 2016, MNRAS, 455, 540
Das, A., Sil, M., Ghosh, R., et al. 2021, FrASS, 8, 78
Das, A., Sil, M., Gorai, P., Chakrabarti, S. I. K., & Loison, J. C. 2018, ApJS, 237, 9
Forest, H., & Dailey, B. 1966, JChPh, 45, 1736
Frisch, M. J., Trucks, G. W., Schlegel, H. B., et al. 2013, Gaussian 09 Revision D.01 (Wallingford CT: Gaussian Inc)
Gadosy, T. A., & McClelland, R. A. 1996, JMoSt, 369, 1
Garrod, R. T. 2008, A&A, 491, 239
Garrod, R. T., Belloche, A., Müller, H. S. P., & Menten, K. M. 2017, A&A, 601, A48

Gómez, I., Rodríguez, E., & Reguero, M. 2006, JMoSt, 767, 11
Gorai, P., Bhat, B., Sil, M., et al. 2020, ApJ, 895, 86
Gorai, P., Das, A., Das, A., et al. 2017a, ApJ, 836, 70
Gorai, P., Das, A., Majumdar, L., et al. 2017b, MolAs, 6, 36
Hasegawa, T. I., Herbst, E., & Leung, C. M. 1992, ApJS, 82, 167
Johnson, R. D., III 1999, NIST 101. Computational Chemistry Comparison and Benchmark Database, Tech. Rep.
Jones, B. M., Zhang, F., Kaiser, R. I., et al. 2011, PNAS, 108, 452
Kojima, T. 1960, JPSJ, 15, 284
Kolesniková, L., Daly, A. M., Alonso, J. L., Tercero, B., & Cernicharo, J. 2013, JMoSp, 289, 13
Larsen, N. W. 1979, JMoSt, 51, 175
Le, H. T., Flammang, R., Gerbaux, P., Bouchoux, G., & Nguyen, M. T. 2001, JPCA, 105, 11582
Lee, K. L. K., Changala, P. B., Loomis, R. A., et al. 2021, ApJL, 910, L2
Lide, D. 2004, CRC Handbook of Chemistry and Physics, Vol. 85 (Boca Raton, FL: CRC Press)
Madronich, S., & Felder, W. 1985, JPhCh, 89, 3556
McCarthy, M. C., Lee, K. L. K., Loomis, R. A., et al. 2021, NatAs, 5, 176
McClellan, A. L. 1963, Tables of Experimental Dipole Moments, Vol. 3 (San Francisco, CA: Freeman)
McGuire, B. A., Burkhardt, A. M., Kalenskii, S., et al. 2018, Sci, 359, 202
McGuire, B. A., Loomis, R. A., Burkhardt, A. M., et al. 2021, Sci, 371, 1265
Møller, C., & Plesset, M. S. 1934, PhRv, 46, 618
Mondal, S. K., Gorai, P., Sil, M., et al. 2021, ApJ, 922, 194
Müller, H. S. P., Belloche, A., Xu, L.-H., et al. 2016, A&A, 587, A92
Olmi, L., Cesaroni, R., & Walmsley, C. M. 1996, A&A, 307, 599
Parker, J. K., & Davis, S. R. 1999, JACS, 121, 4271
Rahul, K. K., Meka, J. K., Pavithraa, S., et al. 2020, AcSpA, 224, 117393
Ravi, V. P., Jasra, R. V., & Bhat, T. S. 1998, JChemTechBiotech, 71, 173
Reese, J. A., Nguyen, T. V., Korter, T. M., & Pratt, D. W. 2004, JACS, 126, 11387
Rolffs, R., Schilke, P., Zhang, Q., & Zapata, L. 2011, A&A, 536, A33
Ruaud, M., Loison, J. C., Hickson, K. M., et al. 2015, MNRAS, 447, 4004
Sahu, D., Das, A., Majumdar, L., & Chakrabarti, S. K. 2015, NewA, 38, 23
Sahu, D., Liu, S.-Y., Das, A., Garai, P., & Wakelam, V. 2020, ApJ, 899, 65
Santoro, D., & Louw, R. 2001, JChemSoc Perkin Transactions, 2, 645
Seta, T., Nakajima, M., & Miyoshi, A. 2006, JPCA, 110, 5081
Shiner, C. S., Vorndam, P. E., & Kass, S. R. 1986, JACS, 108, 5699
Sil, M., Gorai, P., Das, A., Sahu, D., & Chakrabarti, S. K. 2017, EPJD, 71, 45
Sil, M., Gorai, P., Das, A., et al. 2018, ApJ, 853, 139
Sil, M., Srivastav, S., Bhat, B., et al. 2021, AJ, 162, 119
Taatjes, C. A., Osborn, D. L., Selby, T. M., et al. 2010, JPCA, 114, 3355
Tercero, B., Vincent, L., Cernicharo, J., Viti, S., & Marcelino, N. 2011, A&A, 528, A26
Tokmakov, I., & Lin, M.-C. 2002, JPCA, 106, 11309
Turecek, F., Drinkwater, D. E., Maquestiau, A., & McLafferty, F. W. 1989, Organic Mass Spectrometry, 24, 669
Vastel, C., Bottinelli, S., Caux, E., Glorian, J. M., & Boiziot, M. 2015, in SF2A-2015: Proc. Annual Meeting of the French Society of Astronomy and Astrophysics, 313
Vasyunin, A. I., & Herbst, E. 2013, ApJ, 769, 34
Wakelam, V., Smith, I. W. M., Herbst, E., et al. 2010, SSRv, 156, 13
Wang, H., & Frenklach, M. 1997, CoFl, 110, 173
Zhu, L., & Bozzelli, J. W. 2003, JPCA, 107, 3696
Zhu, L., Chen, C.-J., & Bozzelli, J. W. 2000, JPCA, 104, 9197